Heparin Inhibits Cellular Invasion by SARS-CoV-2: Structural Dependence of the Interaction of the Spike S1 Receptor-Binding Domain with Heparin

Courtney J. Mycroft-West[1,*] Dunhao Su[2,*] Isabel Pagani[3,*] Timothy R. Rudd[4,*] Stefano Elli[5,*] Neha S. Gandhi[6,7,*] Scott E. Guimond[8,*] Gavin J. Miller[9] Maria C. Z. Meneghetti[10] Helena B. Nader[10] Yong Li[2] Quentin M. Nunes[11] Patricia Procter[1] Nicasio Mancini[12] Massimo Clementi[12] Antonella Bisio[5] Nicholas R. Forsyth[13] Vito Ferro[14,15] Jeremy E. Turnbull[2,**] Marco Guerrini[5,**] David G. Fernig[2,**] Elisa Vicenzi[3,**] Edwin A. Yates[1,2,**] Marcelo A. Lima[1,**] Mark A. Skidmore[1,2,**]

[1] Molecular and Structural Biosciences, School of Life Sciences, Keele University, Newcastle-Under-Lyme, Staffordshire, United Kingdom
[2] Department of Biochemistry and Systems Biology, Institute of Systems, Molecular and Integrative Biology, University of Liverpool, Liverpool, United Kingdom
[3] Viral Pathogenesis and Biosafety Unit, Division of Immunology, Transplantation and Infectious Diseases, IRCCS San Raffaele Scientific Institute, Milan, Italy
[4] Analytical and Biological Sciences Division, National Institute for Biological Standards and Control, Potters Bar, Hertfordshire, United Kingdom
[5] Istituto di Ricerche Chimiche e Biochimiche G. Ronzoni, Milan, Italy
[6] School of Chemistry and Physics, Queensland University of Technology, Brisbane, Australia
[7] Institute of Health and Biomedical Innovation, Queensland University of Technology, Brisbane, Australia
[8] School of Medicine, Keele University, Newcastle-Under-Lyme, Staffordshire, United Kingdom
[9] School of Chemical and Physical Sciences, Keele University, Newcastle-Under-Lyme, Staffordshire, United Kingdom
[10] Biochemistry Department, Federal University of São Paulo (UNIFESP), São Paulo, SP Brazil
[11] Department of Molecular and Clinical Cancer Medicine, Institute of Systems, Molecular and Integrative Biology, University of Liverpool, Liverpool, United Kingdom
[12] Università Vita-Salute San Raffaele, Milan, Italy
[13] Guy Hilton Research Centre, School of Pharmacy and Bioengineering, Keele University, Hartshill, Stoke-on-Trent, Staffordshire, United Kingdom
[14] School of Chemistry and Molecular Biosciences, The University of Queensland, Brisbane, Australia
[15] Australian Infectious Diseases Research Centre, The University of Queensland, Brisbane, Australia

Address for correspondence Mark A. Skidmore, PhD, Keele University, School of Life Sciences, Huxley Building, Newcastle-Under-Lyme, Staffordshire, ST5 5BG, United Kingdom (e-mail: m.a.skidmore@keele.ac.uk).

Thromb Haemost 2020;120:1700–1715.

Abstract

The dependence of development and homeostasis in animals on the interaction of hundreds of extracellular regulatory proteins with the peri- and extracellular glycosaminoglycan heparan sulfate (HS) is exploited by many microbial pathogens as a means of adherence and invasion. Heparin, a widely used anticoagulant drug, is structurally similar to HS and is a common experimental proxy. Exogenous heparin prevents infection by a range of viruses, including S-associated coronavirus isolate HSR1. Here, we show that heparin inhibits severe acute respiratory syndrome coronavirus-2 (SARS-CoV-2) invasion of Vero cells by up to 80% at doses achievable through prophylaxis and, particularly relevant, within the range deliverable by nebulisation. Surface plasmon resonance and circular dichroism spectroscopy demonstrate that heparin and enoxaparin, a low-molecular-weight heparin which is a clinical anticoagulant, bind and induce a conformational change in the spike (S1) protein receptor-binding domain (S1 RBD) of SARS-CoV-2. A library of heparin derivatives

Keywords

- heparin
- coronavirus
- SARS-CoV-2
- COVID-19
- spike
- S1
- RBD
- circular dichroism
- surface plasmon resonance
- molecular modelling

* These authors are joint first authors.
** Senior authors.

received
June 6, 2020
accepted after revision
October 13, 2020

DOI https://doi.org/10.1055/s-0040-1721319.
ISSN 0340-6245.

and size-defined fragments were used to probe the structural basis of this interaction. Binding to the RBD is more strongly dependent on the presence of 2-*O* or 6-*O* sulfate groups than on *N*-sulfation and a hexasaccharide is the minimum size required for secondary structural changes to be induced in the RBD. It is likely that inhibition of viral infection arises from an overlap between the binding sites of heparin/HS on S1 RBD and that of the angiotensin-converting enzyme 2. The results suggest a route for the rapid development of a first-line therapeutic by repurposing heparin and its derivatives as antiviral agents against SARS-CoV-2 and other members of the *Coronaviridae*.

Introduction

The evolution of multicellular animals required the emergence of networks of interacting extracellular molecules to provide sophisticated communication between cells, underpinning the transition of the unit of natural selection from the individual cell to the entire organism. It is likely that the interactions of the glycosaminoglycans (GAGs) of the peri- and extracellular matrix with proteins were amongst the earliest such molecular networks. For example, choanoflagellates, considered to be extant unicellular descendants of the last common unicellular ancestor of multicellular animals, produce GAGs[1–3] and interactions between their GAGs and a protein from bacterial prey regulate their reproduction.[1,3] In mammals, the GAG heparan sulfate (HS) has the lion's share of protein partners; over 830 extracellular regulatory proteins that bind HS have now been identified.[2,4–6] Numerous pathogens, including parasites, bacteria and viruses exploit the dependence of multicellular organisms on protein–GAG interactions by producing proteins that also bind GAGs.[6,7] The pathogen protein–host GAG interactions are integral to infection, as they are documented to be involved in decoying host cell communication, pathogen adhesion and cell entry.[8,9]

The binding specificity of the interactions of proteins and GAGs, such as HS, depends largely on the complementary spatial disposition of basic groups on the protein and of sulfate and carboxyl groups on the polysaccharide.[4,6,7,10] HS biosynthesis provides a large repertoire of sulfated saccharide sequences and, with sulfation affecting the three-dimensional structure of sugars, a degree of specificity is achieved. This enables cells to differentially bind and respond to extracellular regulatory proteins. The need to accommodate hundreds of protein partners and the redundancy inherent in HS binding sites arising from its biosynthesis makes it difficult to envisage how an organism could enter an evolutionary race with a pathogen by altering protein-binding structures in the polysaccharide. In this light, HS represents an Achilles' heel of organisms with respect to pathogen invasion.

It is, therefore, perhaps not surprising that the list of pathogens exploiting HS is extensive. This includes viruses. Importantly, there appears to be an overlap between the site(s) on viral proteins required for interaction with cell receptors and cell entry, and the site(s) that bind HS. Thus, there is extensive evidence to show that heparin, some of its derivatives and HS inhibit infectivity of a broad spectrum of viruses, including *Coronaviridae* and the severe acute respiratory syndrome (SARS)-associated coronavirus isolate HSR1,[11] flaviviruses,[12,13] herpes,[14] influenza[15] and human immunodeficiency virus.[16,17] Not only does heparin inhibit infectivity of coronavirus isolate HSR1,[11] but there is considerable sequence homology between the receptor-binding domain (RBD) of this *Coronaviridae* and the spike (S1) protein RBD (S1 RBD) of SARS coronavirus-2 (SARS-Cov-2), with basic patches that are likely to interact with heparin overlapping the angiotensin-converting enzyme 2 (ACE2) binding site.

Therefore, we investigated the hypothesis that heparin would both bind the S1 RBD of SARS-CoV-2 and that this interaction would inhibit viral infectivity, using a combination of SARS-CoV-2 plaque assays in Vero cells, surface plasmon resonance (SPR) to establish binding and circular dichroism (CD) spectroscopy to monitor structural changes in the protein following binding. The data demonstrate that heparin does indeed inhibit SARS-CoV-2 infection of Vero cells, and more effectively than for SARS-CoV. Moreover, the S1 RBD binds heparin, as well as the clinical low-molecular-weight heparin, enoxaparin. These interactions elicit a conformational change in the protein; a hexasaccharide being the shortest effective oligosaccharide. The availability, low cost and clinical grade of heparin, HS and derivatives, as well as the fact that they are safe to administer to patients in critical care, make these polysaccharides attractive first-line therapeutic candidates for viral diseases such as COVID-19 and could, perhaps, contribute to a prophylactic control strategy.

Methods

Vero Cell Culture and Assays

African green monkey Vero kidney epithelial cells were purchased from ECACC and maintained at 50 to 75% confluence in DMEM (Gibco, United Kingdom), supplemented with 10% (v/v) foetal calf serum (SLS, United Kingdom), 20 mM L-glutamine (Gibco, United Kingdom), 100 U mL^{-1} penicillin-G (Gibco, United Kingdom) and 100 U mL^{-1} streptomycin sulfate (Gibco, United Kingdom), with 5% CO_2 at 37°C.

For cellular invasion assays, Vero cells were plated at 2.5×10^5 cells per well in 24-well plates and incubated with EMEM (Sigma-Aldrich, Italy) supplemented with 10% (v/v) foetal calf serum (complete medium). Twenty four hours later, cells were incubated with porcine mucosal heparin (6.25–200 µg mL^{-1}; Celsus Laboratories, Cincinnati, United States) in 300 µL of complete medium, 1 hour prior to infection and then incubated with virus solution containing 50 plaque forming

units (PFUs) of either Italy/UniSR1/2020 isolate (GISAID accession ID: EPI_ISL_413489[18] or, SARS-CoV HSR-1 (EID 2004). After incubation for 1 hour at 37°C, supernatants were discarded and 500 µL of 1% (w/v) methylcellulose (Sigma-Aldrich, Italy) overlay (in complete medium) were added to each well. After 3 days, cells were fixed using a 6% (v/v) formaldehyde: phosphate-buffered saline (PBS) solution and stained with 1% (w/v) crystal violet (Sigma-Aldrich, Italy) in 70% (v/v) methanol (Sigma-Aldrich, Italy). The plaques were counted using a stereoscopic microscope (SMZ-1500, Nikon).

For RBD-binding assays, Vero cells were plated into 96-well cell culture plates at 1,000 cells per well in 100 µL of in DMEM supplemented with 10% (v/v) foetal calf serum, 20 mM L-glutamine, 100 U mL^{-1} penicillin-G and 100 U mL^{-1} streptomycin sulfate, and were allowed to adhere overnight. Medium was aspirated prior to washing thrice with 200 µL of 1× PBS (CMF-PBS; Ca^{2+} and Mg^{2+} free; Lonza, United Kingdom). Cells were fixed with 100 µL of 10% neutral buffered formalin (Thermo Fisher, United Kingdom) for 10 minutes at room temperature. Wells were washed thrice with 200 µL of CMF-PBS. Then 100 µL CMF- PBS was added to each well and plates were stored at 4°C until use. Prior to binding assays, wells were blocked with 200 µL CMF-PBS + 1% (w/v) bovine serum albumin (BSA; Sigma-Aldrich, United Kingdom) for 1 hour at room temperature, washed thrice with 200 µL CMF-PBS with 0.1% (v/v) Tween-20 (PBST, Sigma-Aldrich, United Kingdom) followed by two washes with 200 µL of CMF-PBS. SARS-CoV-2 S1 RBD (50 µg mL^{-1}) with or without heparin (100 µg mL^{-1}) were added to each well with 25 µL PBST + 0.1% (w/v) BSA prior to incubation for 1 hour at room temperature, while rocking. Post incubation, wells were washed thrice with 200 µL PBST and twice with 200 µL CMF-PBS before incubation (with agitation) for 1 hour at room temperature, under dark conditions with an Alexa Fluor 488 anti-his tag antibody (clone J095G46, Biolegend, United Kingdom) 1:5,000 (v/v) in 25 µL PBST with 0.1% (w/v) BSA per well. Wells were washed thrice with 200 µL PBST and twice with 200 µL CMF-PBS. Fluorescence emission was measured using a Tecan Infinite M200Pro plate reader ($\lambda_{ex.} = 495$ nm, $\lambda_{em.} = 520$ nm) with results presented as the mean ± the standard deviation ($n = 3$).

Expression and Purification of Recombinant SARS-CoV-2 S1 RBD

Residues 330 – 583 of the SARS-CoV-2 spike protein (GenBank: MN908947) were cloned upstream of an N-terminal 6xHis-tag in the pRSETA expression vector and transformed into SHuffle T7 Express Competent *E. coli* (NEB, United Kingdom). Protein expression was performed in MagicMedia *E. coli* Expression Media (Invitrogen, United Kingdom) at 30°C for 24 hours, 250 rpm. The bacterial pellet was suspended in 5 mL of lysis buffer (BugBuster Protein Extraction Reagent, Merck Millipore, United Kingdom; containing DNAse) and incubated at room temperature for 30 minutes. The protein was purified from inclusion bodies using immobilized metal affinity chromatography under denaturing conditions. On-column protein refolding was performed by applying a gradient with decreasing concentrations of the denaturing agent (6 to 0 M urea). After extensive washing, protein was eluted using 20 mM NaH_2PO_4, pH 8.0, 300 mM NaCl, 500 mM imidazole. Fractions were pooled and buffer-exchanged to PBS (140 mM NaCl, 5 mM NaH_2PO_4, 5 mM Na_2HPO_4, pH 7.4; Lonza, United Kingdom) using a Sephadex G-25 column (GE Healthcare, United Kingdom). Recombinant protein was stored at −20°C until required.

Preparation of Chemically Modified Heparin Derivatives

All chemically modified heparin polysaccharides (►**Table 1**) were synthesised from parental unfractionated porcine mucosal heparin ($M_w = 12$ kDa; Celsus Laboratories, Cincinnati, United States) as previously described.[15,19] The veracity of all chemical modifications was ascertained using ^1H and ^{13}C NMR, with chemical shifts compared with TSP (Sigma-Aldrich, United Kingdom) as an external reference standard.

Secondary Structure Determination of SARS-CoV-2 S1 RBD by Circular Dichroism Spectroscopy

The CD spectrum of the SARS-CoV-2 S1 RBD in PBS was recorded using a J-1500 Jasco CD spectrometer (Jasco, United Kingdom), Spectral Manager II software (JASCO, United Kingdom) and a 0.2-mm path length, quartz cuvette (Hellma, United States) scanning at 100 nm min^{-1} with 1 nm resolution throughout the range of 190 to 260 nm. All spectra obtained were the mean of five independent scans, following

Table 1 Repeating disaccharide structures of heparin derivatives

	R1	R2	R3	
Heparin 1	SO_3^-	SO_3^-	SO_3^-	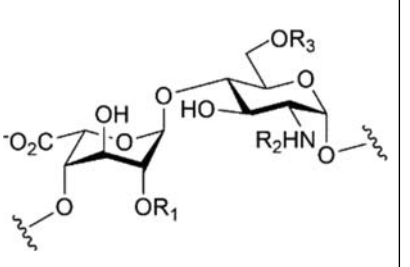
Heparin 2	SO_3^-	$COCH_3$	SO_3^-	
Heparin 3	H	SO_3^-	SO_3^-	
Heparin 4	SO_3^-	SO_3^-	H	
Heparin 5	H	$COCH_3$	SO_3^-	
Heparin 6	SO_3^-	$COCH_3$	H	
Heparin 7	H	SO_3^-	H	
Heparin 8	H	$COCH_3$	H	
Heparin 9[a]	SO_3^-	SO_3^-	SO_3^-	

[a]Additionally, chemically O-sulfated at positions C-3 of glucosamine and C-3 of the uronic acid.

instrument calibration with camphorsulfonic acid. SARS-CoV-2 S1 RBD was buffer-exchanged (prior to spectral analysis) using a 5 kDa Vivaspin centrifugal filter (Sartorius, Germany) at 12,000 g thrice and the CD spectra were collected using 21 µL of a 0.6 mg mL^{-1} solution in PBS, pH 7.4. Spectra of heparin (porcine mucosal heparin), its derivatives and oligosaccharides were collected in the same buffer at approximately comparable concentrations, since these are polydisperse materials. Collected data were analysed with Spectral Manager II software prior to processing with GraphPad Prism 7, using second-order polynomial smoothing through 11 neighbours. Secondary structural prediction was calculated using the BeStSel analysis server.[20] To ensure that the CD spectral change of SARS-CoV-2 S1 RBD in the presence of porcine mucosal heparin did not arise from the addition of the heparin alone, which is known to possess a CD spectrum at high concentrations,[21,22] a difference spectrum was analysed. The theoretical CD spectrum, which resulted from the arithmetic addition of the CD spectrum of the SARS-CoV-2 S1 RBD and that of the heparin, differed from the observed experimental CD spectrum of SARS-CoV-2 S1 RBD mixed with heparin. This demonstrates that the change in the CD spectrum arose from a conformational change following binding to porcine mucosal heparin.

Surface Plasmon Resonance Determination of SARS-CoV-2 S1 RBD Binding to Unfractionated Heparin

Human fibroblast growth factor 2 (FGF2) was produced as described by Duchesne et al.[23] Porcine mucosal heparin was biotinylated at the reducing end using hydroxylamine biotin (Thermo Fisher, United Kingdom) as described by Thakar et al.[24] Heparin (20 µL of 50 mg mL^{-1}) was reacted with 20 µL of hydroxylamine biotin in 40 µL of 300 mM aniline (Sigma-Aldrich, United Kingdom) and 40 µL, 200 mM acetate pH 6 for 48 hours at 37°C. Free biotin was removed by gel-filtration chromatography on Sephadex G25 (GE Life Sciences, United Kingdom).

A P4SPR, multi-channel SPR instrument (Affinté Instruments; Montréal, Canada) was employed. The functionalisation of the gold sensor surface was a modification of a described method.[25] Briefly, a gold sensor chip that was plasma-cleaned prior to derivatisation: a self-assembled monolayer of polyethylene glycol methyl ether (mPEG) thiol and biotin mPEG was formed by incubating the chip in a 1 mM solution of these reagents at a 99:1 molar ratio in ethanol for 24 hours. The chip was rinsed with ethanol and placed in the instrument. PBS was used as the running buffer for the three sensing channels and a fourth background channel at 500 µL min^{-1}, using an Ismatec pump. Twenty micrograms of streptavidin (Sigma, United Kingdom; 1 mL in PBS) was injected over the four channels. Subsequently, biotin–heparin (1 mL) was injected over the three measurement channels, the fourth serving as a control.

Binding experiments were performed using PBS with 0.02% (v/v) Tween 20 as the running buffer. The ligand was injected over the three sensing channels after dilution to the concentration indicated in the figure legends, at 500 µL min^{-1}. Sensor surfaces with bound FGF2 were regenerated using a wash of 2 M NaCl (Fisher Scientific, United Kingdom); however, this was found to be ineffectual for SARS-CoV-2 S1 RBD. Partial regeneration of the surface was achieved with 20 mM HCl (VWR, United Kingdom), although only 0.25% (w/v) SDS (VWR, United Kingdom) was found to remove the bound SARS-CoV-2 S1 RBD protein. After regeneration with 0.25% (w/v/) SDS, fluidics and surfaces were washed with 20 mM HCl to ensure all traces of detergent were removed. Background binding to the underlying streptavidin bound to the mPEG/biotin mPEG self-assembled monolayer was determined by ligand injection over the control channel. Responses are reported as the change in plasmon resonance wavelength (nm) and for the three control channels represent their average response. Reliable kinetic parameters could not be calculated since the data for interactions involve several potential binding sites in the ligand and mass transport artefacts associated with flow systems meant that the data did not fit a single site model.

Prediction of SARS-CoV-2 S1 Heparin-Binding Domain

The methods employed to predict heparin-binding sequences within the SARS-CoV-2 S1 RBD are described in Rudd et al.[6]. A brief description of the method follows. In combination, Ori et al[2] and Nunes et al[5] identified 786 heparin-binding proteins. In this study, 776 heparin-binding proteins, from the previously identified list, were decomposed into amino acid sequences containing no less than three residues with at least one basic amino acid. To simplify the problem, the heparin-binding proteins were fragmented into sequences containing the following combinations of amino acids: BX, BXA, BXS, BXP, BXAS, BXAP and BXPS (where, B = basic, X = hydrophobic, A = acidic, P = polar and S = special). These sequences were compared using a metric based on the Levenshtein distance, a measure of the similarity between strings of characters, which is based on the minimum number of insertions, deletions or substitutions that need to be applied to the characters to alter one sequence so that it matches the other. Sequences with a similarity score of greater than 0.7 (70% similarity) were considered highly conserved. These sets of highly conserved basic amino acid containing sequences found in heparin-binding proteins were then used to identify possible heparin-binding sequences within SARS-CoV-2 S1, utilising the same Levenshtein similarity cut-off of 0.7.

Molecular Docking and Molecular Dynamics Simulations of Heparin-SARS-CoV-2 RBD Domain

The in silico docking of heparin binding to the spike RBD based on the crystal structure 6LZG (residues 333–527)[26] was performed using the ClusPro server version 2.0 that includes an advanced option for heparin tetrasaccharide docking. At the time of this work, another crystal structure was released (PDB code: 6M0J).[27] Both RBD structures (PDB: 6LZG and 6M0J) are superimposed with a root mean square deviation of 0.6Å and have similar interactions with ACE2. Therefore, for this work, molecular modelling was performed on the spike RBD chain (PDB code: 6LZG) after removing the ACE2 domain. In alignment with the protein sequence used in this experimental work, we also performed modelling of heparin oligosaccharides on the structure (PDB: 6ZGG; chain B) containing both RBD and SD1 domains (residues 330 −583).

ClusPro is a fast and crude approach to predict heparin-binding sites on the protein surface using generic

tetrasaccharides; however, it cannot capture the flexibility and structural variability of longer oligosaccharides (greater than tetrasaccharides) with sulfated and acetylated regions that might be involved in protein binding. Therefore, docking calculations of heparin hexasaccharide and octasaccharide ligands (containing the trisulfated disaccharide sequence; Heparin 1) to spike RBD were performed using the GlycoTorch Vina program.[28] These model ligands were built using the Glycam server. The protein and ligands were then converted to appropriate file formats for docking using the GlycoTorch tools. The binding sites on the protein surface were defined based on the output from the ClusPro heparin docking analysis. The docked poses obtained from docking studies on sites I and III were subjected to the molecular dynamics (MD) simulations.

To investigate the conformational changes in the protein–heparin complex in the presence of explicit solvent, classical MD simulations using the AMBER simulation package were performed on the heparin hexasaccharide–RBD complex (site III) and heparin octasaccharide–RBD (site I) complex. AMBER ff99SB*-ildn[29] and GLYCAM (version 06j1)[30] force fields were used for protein and heparin, respectively. The systems consisting of the protein–heparin complex were solvated using TIP3P solvent[31] in an octahedral box by keeping a minimum distance of 12.0 Å between each face of the box and the complex in both cases. Sodium and chloride ions were added to obtain 0.15 M ionic strength, as well as to neutralise the charges. The AMBER16 pmemd.cuda[32] module was used to perform MD simulations. The system preparation consisted of four steps. In the first step the solvent and the ions were relaxed in a 2,000-step steepest descent energy minimisation with the protein–heparin position restrained using a force constant of 10 kcal/mol·Å^2. A further step of energy minimisation was performed with the position restraints removed (500 steps of steepest descent and 1,500 steps of conjugate gradient minimisation). After minimisation, the system was heated to $T = 298$ K in a 100 ps Langevin dynamics simulation under NVT conditions with restraints on protein–heparin using a force constant of 10 kcal/mol·Å^2, followed by a 2 nanosecond NPT simulation using a Berendsen barostat and a force constant of 2 kcal/mol·Å^2 on protein–heparin. A further 2 nanosecond NPT unrestrained simulation was performed for the density equilibration of the system. The production runs were performed for 500 nanoseconds using a Langevin dynamics integrator under constant pressure ($p = 1$ bar) and temperature ($T = 298$ K), with a time step of 2 fs. Long-range electrostatic calculations were performed using the PME method. Heavy atom–hydrogen bonds were constrained using SHAKE. A cutoff of 12.0 Å was applied to van der Waals forces. Periodic boundary conditions were applied throughout.

Visualisation of the molecular models was performed using UCSF Chimera.[33] Molecular surfaces coloured by electrostatic potential were generated using APBS and PDB2PQR[34] web servers with a protein interior dielectric constant of 2, a solvent dielectric constant of 78.54. To obtain more detailed information about the contribution of binding residues, the MM/GBSA module of AMBER 16.0[32] was used to compute the per-residue energy decompositions for every individual frame, adding 1 to 4 energy terms to internal energy terms; the energies for every residue were averaged over the 50,000 frames of production dynamics. The polar component of the desolvation energy was determined via Onufriev's GB (igb = 5)[35] and the nonpolar contribution was estimated based on the solvent-accessible surface area using the LCPO method[36] implemented in Amber. MM/GBSA calculations were performed using mbondi2 radii and default settings for the nonpolar decomposition scheme, surface tension, and cavity offset, whereas the ionic strength was changed from 0.0 to 0.150 M to be consistent with MD simulations in explicit solvent. The outer dielectric and solute dielectric constants were set to 80 and 1, respectively. More details of the MM/PB(GB)SA methods can be found in the literature.[37]

Results

SARS-CoV-2 Viral Plaque-Forming Assays and RBD Binding

The titer of infectious virions was measured using standard plaque-forming assays on Vero cells with and without a heparin pre-treatment (from 200 µg mL^{-1}, 1 hour prior to infection) with both a historical SARS-CoV isolate HSR-1 and the recent SARS-CoV-2 isolate, Italy/UniSR1/2020. Significant decreases were observed in the number of PFU upon heparin treatment for both SARS-CoV and SARS-CoV-2, with the latter demonstrating significantly higher levels of inhibition (80%) than for SARS-CoV (►**Fig. 1**). Vero cells have the advantage that they are defined and well-characterised and, when infected by viruses, do not secrete α- or β-interferon. Heparin treatment was also able to inhibit the SARS-CoV-2 RBD binding to the cell surface of Vero cells (►**Fig. 1B**) The observed inhibition may be due to direct competition of the exogenous heparin for host cell surface GAGs and/or for the ACE2 receptor and demonstrates that addition of exogenous heparin can disrupt the interaction of the virus with the cell. It is noteworthy that the heparin concentrations used cover both prophylactic and therapeutic heparin nebulisation protocols,[38] highlighting that this in vitro regime correlates with heparin use clinically, which is not the case for some of the other drugs tested thus far against COVID, e.g. ivermectin.[39]

Surface Plasmon Resonance Binding Studies

Fibroblast growth factor 2, a well-characterised heparin-binding protein, was used to confirm the successful functionalisation of the three sensing channels with biotin–heparin. Injection of 1 mL 100 nM FGF2 over the sensing channels elicited a significant response (►**Fig. 2A**, injection between the blue and red arrows). However, 100 nM FGF2 elicited no response in the control channel, functionalised solely with streptavidin (►**Fig. 2A**). The bound FGF2 was removed by a wash with 2 M NaCl, as previously for the IASys optical biosensor.[40]

When 800 nM SARS-CoV-2 S1 RBD was injected over the three sensing channels, there was an increase in the signal of binding (►**Fig. 2B** injection starts at the blue arrow). At the end of the injection, the system returned to the running buffer (PBST, red arrow). There was no dissociation. This is common in surface measurement, particularly in flow systems, due to the extensive boundary layer[41] of liquid enabling rebinding of the analyte and often causes a substantial underestimation of the

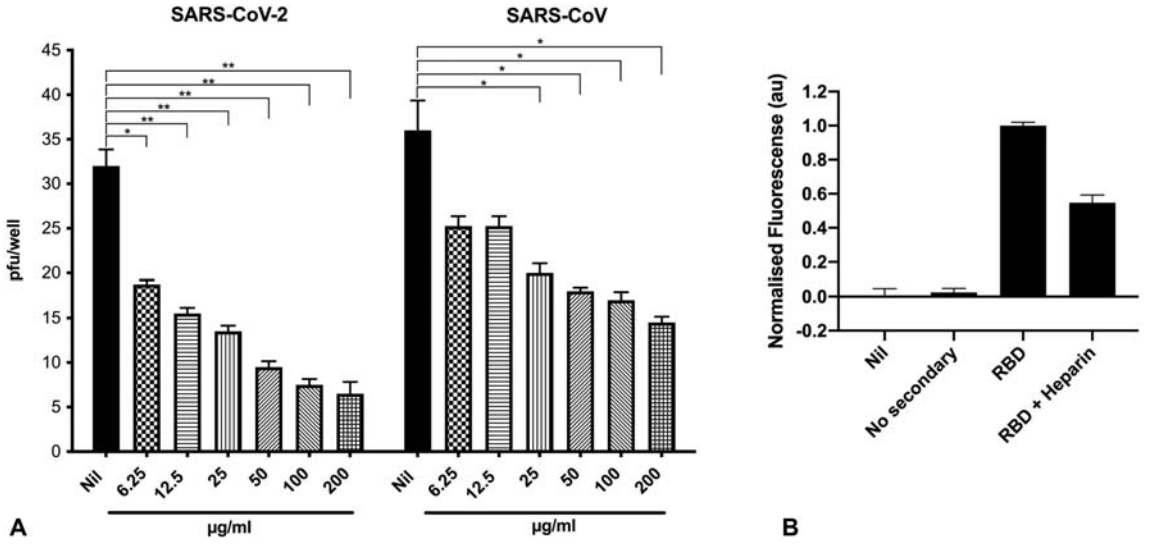

Fig. 1 The heparin-mediated inhibition of SARS-CoV-2 viral invasion of Vero cells. (**A**) The effect of unfractionated porcine mucosal heparin added 1 hour before the infection of Vero cells with 50 PFU of SARS-CoV-2 or SARS-CoV. The results are expressed as the number of PFU per well and represent the mean ± SD of quadruplicate cultures. The *p*-value was calculated using the Mann–Whitney U test, $^{*}P \leq 0.05$; $^{**}P \leq 0.01$; $^{***}P \leq 0.001$. (**B**) The effect of unfractionated porcine mucosal heparin (100 µg mL^{-1}) on RBD binding to Vero cells. Nil represents no treatment; no secondary represents no secondary antibody control; au, arbitrary units of fluorescence. PFU, plaque-forming unit; RBD, receptor-binding domain; SD, standard deviation.

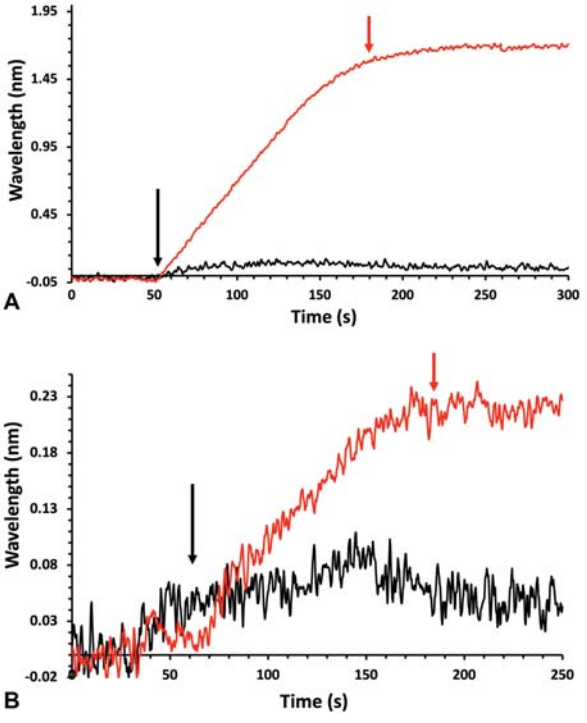

Fig. 2 Interaction of FGF2 and 800 nM SARS-CoV-2 S1 RBD with immobilised heparin. Reducing end biotinylated heparin was immobilised on a streptavidin-functionalised P4SPR sensor surface [no biotin-heparin (–) control]. PBS running buffer flow rate was 500 µL min^{-1}. The data for the three sensing channels are reported as an average response (–). The start of protein injections is indicated by *black arrows* and the return of the surface to the running buffer (PBST) by *red arrows*. (**A**) Injection of 100 nM FGF2. (**B**) Injection of 800 nM SARS-CoV-2 S1 RBD protein. PBS, phosphate buffered saline; PBST, phosphate buffered saline with Tween-20; RBD, receptor-binding domain.

dissociation rate, k_{off}, which can be remedied by the addition of soluble ligand.[42] The injection of 800 nM SARS-CoV-2 S1 RBD over the control channel, functionalised with just streptavidin, showed a small increase in response (►**Fig. 2B**) of the order of 10% of that seen in the measurement channel. Repeated measurements indicate that this is the maximum level of background binding. These data demonstrate that 800 nM SARS-CoV-2 S1 RBD binds specifically to heparin immobilised through its reducing end and does not interact extensively with the underlying streptavidin/ethylene glycol surface. It should be noted that when biotin–heparin is anchored to the streptavidin layer, as in the measurement channels, such background binding will be reduced, since less of the underlying surface is exposed. This is illustrated in the competition experiments, in which soluble heparin was able to completely abrogate the binding of SARS-CoV-2 S1 RBD to the surface (►**Fig. 3A**).

In a first set of competition experiments, 800 nM SARS-CoV-2 S1 RBD was mixed with heparin or enoxaparin at the indicated concentration and injected over the sensing channels. The response when the surface returned to the running buffer, PBST, was then measured. This is appropriate, since there is no appreciable dissociation of the heparin-bound SARS-CoV-2 S1 RBD when the surface returns to PBST (►**Fig. 2B**) and it ensures that any differences in refractive index of the samples do not interfere with the measurement. At 1.7 µg mL^{-1} heparin, a small reduction in the binding of SARS-CoV-2 S1 RBD was observed (►**Fig. 3A**) and, as the concentration of heparin increased, the binding of SARS-CoV-2 S1 RBD decreased in a dose-dependent manner. SARS-CoV-2 S1 RBD binding was completely abrogated by 1.7 mg mL^{-1} heparin. The low-molecular-weight heparin, enoxaparin, was also found to inhibit the binding of SARS-CoV-2 S1 RBD, but on a weight basis it was less potent than heparin (►**Fig. 3A**). Thus, a small inhibition of binding was observed at 17 µg/mL enoxaparin and the maximal inhibition observed with this polysaccharide was 70% at 1.7 mg mL^{-1}. These data indicate that heparin is approximately 30-fold more potent an inhibitor of the interaction of SARS-CoV-2 S1 RBD with immobilised heparin than enoxaparin. We then examined whether short oligosaccharides

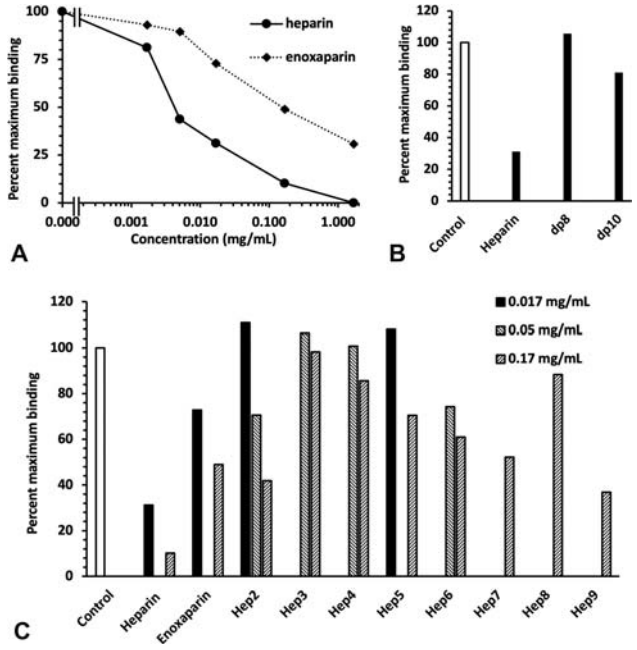

Fig. 3 Competition for SARS-CoV-2 S1 RBD binding to immobilised heparin with model heparin-derived oligo- and polysaccharides. 800 nM SARS-CoV-2 S1 RBD was injected onto the surface in the presence or absence of the indicated concentration of heparin-derived oligo- and polysaccharides. Since the SARS-CoV-2 S1 RBD does not dissociate appreciably when the system returns to PBST, this is when the response was measured, to avoid any confounding effects of differences of refractive index between samples. A control measurement (800 nM SARS-CoV-2 S1 RBD alone) was performed before each competition and used to calculate the percentage of maximum binding. This ensured that small changes over time in the responsiveness of the surface did not confound the analysis. (**A**) Competition for 800 nM SARS-CoV-2 S1 RBD binding to immobilised heparin by heparin and by enoxaparin. (**B**) Competition for 800 nM SARS-CoV-2 S1 RBD binding to immobilised heparin by 0.17 mg mL^{-1} heparin-derived dp 8 and dp 10, with the corresponding value for heparin from panel (A) shown to aid comparison. (**C**) Competition for 800 nM SARS-CoV-2 S1 RBD binding to immobilised heparin by a panel of orthogonally chemically desulfated heparins (►**Table 1**). PBST, phosphate buffered saline with Tween-20; RBD, receptor-binding domain.

could inhibit SARS-CoV-2 S1 RBD binding. A heparin-derived octasaccharide (dp 8) was without effect, but a decasaccharide (dp10) at 0.17 mg mL^{-1} showed a modest inhibition of SARS-CoV-2 S1 RBD binding to immobilised heparin (►**Fig. 3B**). Whether these data reflect a true requirement for a longer structure for SARS-CoV-2 S1 RBD binding or instead relate to selective reduction in the presence of particular binding structures in the polysaccharide as a consequence of the manufacturing processes employed (β-elimination for enoxaparin and partial enzymatic heparin degradation for oligosaccharides) remains to be determined.

The ability of a library of heparins that had been selectively modified (►**Table 1**) to inhibit SARS-CoV-2 S1 RBD binding was determined. This showed different levels of inhibitory activity, depending on their pattern of sulfation. Of the singly desulfated heparins, heparin 2 (►**Table 1**), which is de-*N*-sulfated/*N*-acetylated, showed inhibitory activity at 0.05 and 0.17 mg mL^{-1}, whereas heparin 3 and heparin 4 (►**Table 1**), which are de-*O*-sulfated at C-2 and C-6, respectively, had no detectable inhibitory activity (►**Fig. 3C**). This suggests that SARS-CoV-2 S1 RBD has a preference for regions of saccharides that are 2-*O*- and 6-*O*-sulfated. Interestingly, the doubly desulfated heparins (heparin 5, heparin 6, heparin 7; ►**Table 1**) possessed inhibitory activity, albeit lower than the native heparin (►**Fig. 3C**). Since the sulfation of the polysaccharide has a marked effect on its conformation,[43] these data suggest that the SARS-CoV-2 S1 RBD may have a preference for a particular spatial arrangement of charged groups. Completely desulfated heparin (heparin 8) had no inhibitory activity, indicating that ionic interactions with sulfate groups make an important contribution to the interaction of the SARS-CoV-2 S1 RBD with the polysaccharide. Over-sulfated heparin (heparin 9) inhibited most strongly of the heparin derivatives, but not as effectively as native heparin. This highlights the likely importance of polysaccharide conformation for SARS-CoV-2 S1 RBD binding, since sulfation on all available hydroxyls renders the polysaccharide more rigid and restricts its conformational flexibility.[43,44]

Secondary Structure Determination of SARS-CoV-2 S1 RBD Protein by Circular Dichroism Spectroscopy

Circular dichroism spectroscopy in the far-ultraviolet region (190–260 nm) detects conformational changes in protein secondary structure that occur in solution and can also infer binding by an added ligand. The SPR data showed that there is binding between heparins and SARS-CoV-2 S1 RBD, whereas the CD spectra would indicate whether this binding interaction was accompanied by changes in secondary structure in the protein. Such structural changes can be quantified using deconvolution of the CD spectra.[45] SARS-CoV-2 S1 RBD underwent conformational change in the presence of heparin (►**Figs. 4** and **5**), consisting of an increase in α-helix content of 1.5% and a decrease in global β-sheet of 2.1%. The observed changes demonstrate that when the SARS-CoV-2 S1 RBD interacts with heparin in aqueous conditions of physiological relevance, it undergoes conformational change. A chemically modified heparin derivative with the predominant repeating disaccharide structure, IdoA-GlcNAc,6S (heparin 5), was able to induce closely comparable secondary structural changes in the SARS-CoV-2 S1 RBD as heparin (►**Fig. 5A–C**; ►**Supplementary Fig. S1** [available in the online version]). Analysis by CD spectroscopy of the role of chain length for heparin-derived oligosaccharides (►**Fig. 6A–D**) revealed that a hexasaccharide fraction was able to induce similar conformational changes to heparin even though small heparin oligosaccharides were not effective inhibitors in the SPR experiments. Together, the data show that although there is an apparent dependence on size and charge for the binding of SARS-CoV-2 S1 RBD with polysaccharides, the structure–function relationship seems to be more complex. It is also important to note that heparin and its derivatives are produced by methods designed to enrich anticoagulant properties, making it difficult to propose antiviral structure–function studies without proper selection based on the actual antiviral properties of heparin.

Heparin-Binding Site Analysis

Interactions with basic amino acids are known to dominate the binding between proteins and heparin. With that in mind, primary sequence analysis of the expressed protein domain and analysis of the modelled SARS-CoV-2 S1 RBD structure

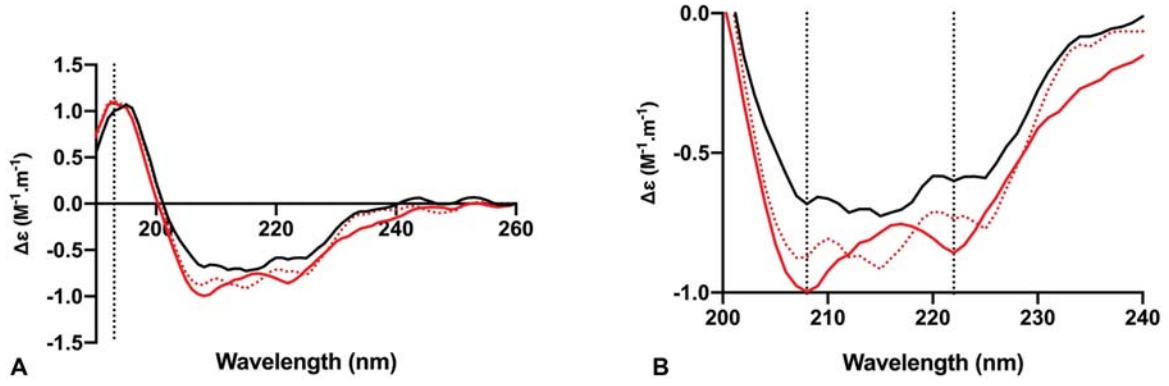

Fig. 4 The conformational change of the SARS-CoV-2 S1 RBD observed in the presence of heparin by CD spectroscopy. (**A**) Circular dichroism spectra (190–260 nm) of SARS-CoV-2 S1 RBD alone (*black solid line*) and with heparin (*red solid line*) in PBS, pH 7.4. The *red, dotted line* represents the sum of the two individual spectra and the fact that this is distinct from the spectrum of the RBD with heparin (*red solid line*) indicates that a conformational change and, therefore, binding have occurred. The *dotted vertical line* indicates 193 nm. (**B**) Details of the same spectra expanded between 200 and 240 nm. *Vertical dotted lines* indicate 222 and 208 nm. PBS, phosphate buffered saline; RBD, receptor-binding domain.

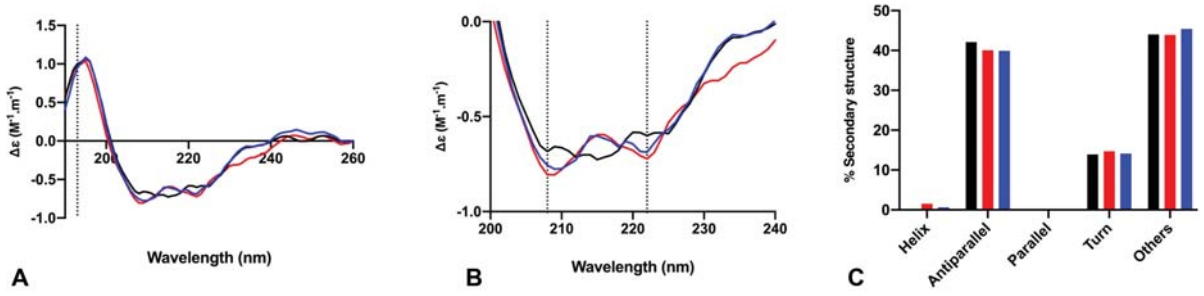

Fig. 5 The conformational change of the SARS-CoV-2 S1 RBD observed in the presence of a chemically modified heparin derivative by CD spectroscopy. (**A**) Circular dichroism spectra (190–260 nm) of SARS-CoV-2 S1 RBD alone (*black solid line*) with heparin (*red solid line*) and with a chemically modified derivative, heparin 5 (►**Table 1**), with the predominant repeating disaccharide structure; –IdoA2OH-GlcNAc6S–(*blue solid line*) in PBS, pH 7.4. The *vertical dotted line* indicates 193 nm (**B**). The same spectra expanded between 200 and 240 nm. *Vertical dotted lines* indicate 222 and 208 nm. (**C**) Secondary structure content analysed using BeStSel (20) for SARS-Cov-2 S1 RBD [analysis using BeStSel was performed on smoothed CD data from (A) between 190 and 260 nm]. PBS, phosphate buffered saline; RBD, receptor-binding domain.

(►**Fig. 7**) were conducted, which indicated that there are several potential heparin-binding sites and, importantly, these patches of basic amino acids are exposed on the protein surface.

Analysis of the RBD sequence for potential heparin-binding sites employing a metric based on the Levenshtein distance (a measure of the similarity between two sequences) found that the basic amino acid sequences within SARS-CoV-2 S1 RBD were similar to 278 sequences found in 309 heparin-binding proteins. The predicted heparin-binding basic amino acid sequences are shown in ►**Tables 2** and **3**. Basic amino acids with a normalised count greater than 0.5 were found at: RKR 355–356 (0.941), LVK 533–535 (1.00), KK 557–558 (0.544) and R 557 (0.688). There were also several possible secondary sites of interaction (a normalised count greater than 0.3): R 346 (0.368), R 403 (0.386), K 417 (0.309) and H 519 (0.305). One consequence of the ability of SARS-CoV-2 S1 RBD to interact with HS is that it may provide a route for adhering to cell surfaces, enabling invasion. Conversely, this region also interacts with the orthodox receptor of the spike protein ACE2 (SARS-CoV-2 S1 RBD 436–529), suggesting that heparin and its derivatives interfere with the interactions between the virus, via these residues. Furthermore, most of the identified sequences, with three exceptions [TKLN (385–389), GKIADYNYKLP (416–427) and PYRVVVL (507–514)], are exposed on the protein surface and available for binding.

Studying SARS-CoV-2 spike protein structure and behaviour in solution is an important step in the development of effective therapeutics against SARS-CoV-2. Here, the ability of the SARS-CoV-2 S1 RBD to bind pharmaceutical heparin, studied using spectroscopic techniques, showed that SARS-CoV-2 S1 RBD binds to heparin and that, upon binding, a significant conformational change is induced. Moreover, moieties of basic amino acid residues that are common constituents of heparin-binding domains, and accessible to solvent, are present on the SARS-CoV-2 S1 RBD surface, forming a series of continuous patches (►**Fig. 7**), suitable for heparin binding.

Comparison of the RBD amino acid sequence (residues 330–583) with an extensive library of sequences from known heparin-binding proteins (►**Tables 2** and **3**) based on the *Levenshtein distance,* which provides a measure of the degree of similarity between the sequences, suggests that wider areas of the RBD surface may be available (►**Fig. 7**) for binding to host cell surface GAGs, which can be disrupted by heparin (►**Fig. 1B**). These may relate to the propensity for the virus to select particular species, individuals, age groups and cell types, since the GAG composition is known to vary with these different parameters. There is also evidence of a potential heparin-binding gain of function mutation (T346R) from Bat-RaTG13 (►**Fig. 7**).

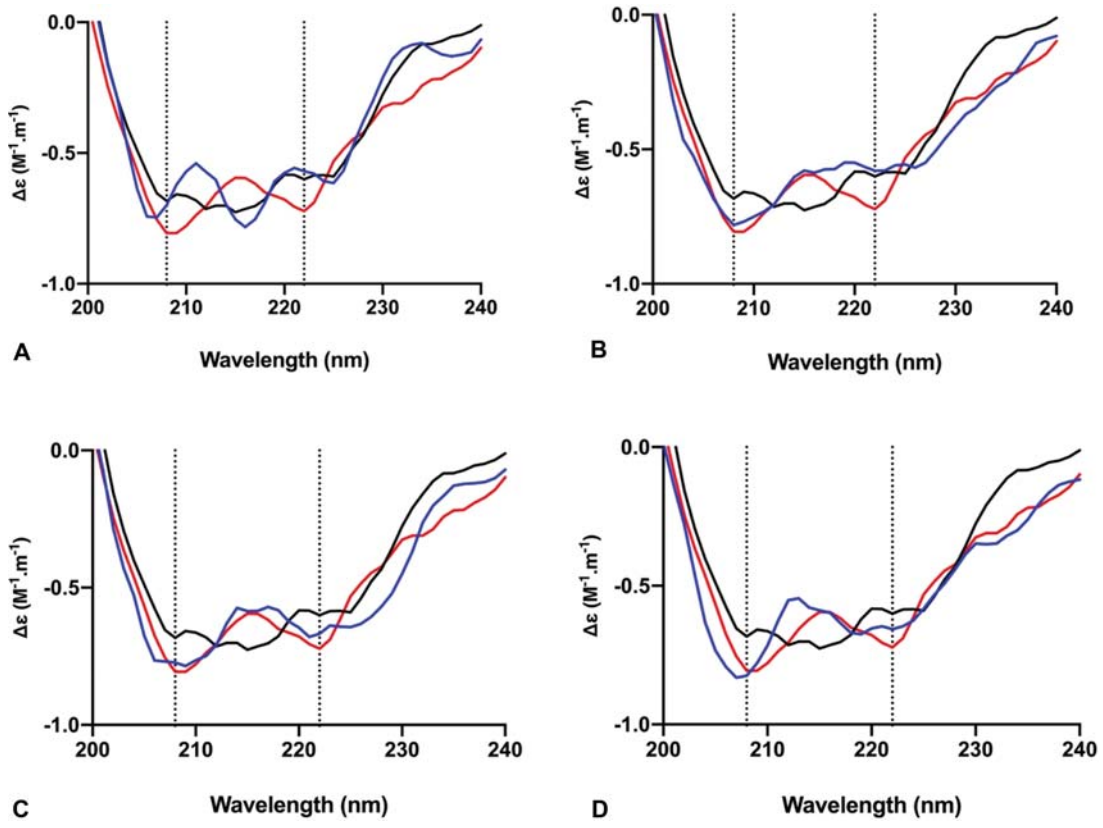

Fig. 6 The conformational change of the SARS-CoV-2 S1 RBD observed in the presence of size-defined heparin oligosaccharides by CD spectroscopy. Circular dichroism spectra between 200 and 240 nm of SARS CoV-2 S1 RBD in PBS, pH 7.4, alone (*black solid line*), with heparin (*red solid line*), and PMH-derived, size-defined oligosaccharides (*blue solid line*): (**A**) Tetrasaccharide, (**B**) hexasaccharide, (**C**) octasaccharide, and (**D**) decasaccharide. *Vertical dotted lines* indicate 222 and 208 nm. PBS, phosphate buffered saline; RBD, receptor-binding domain.

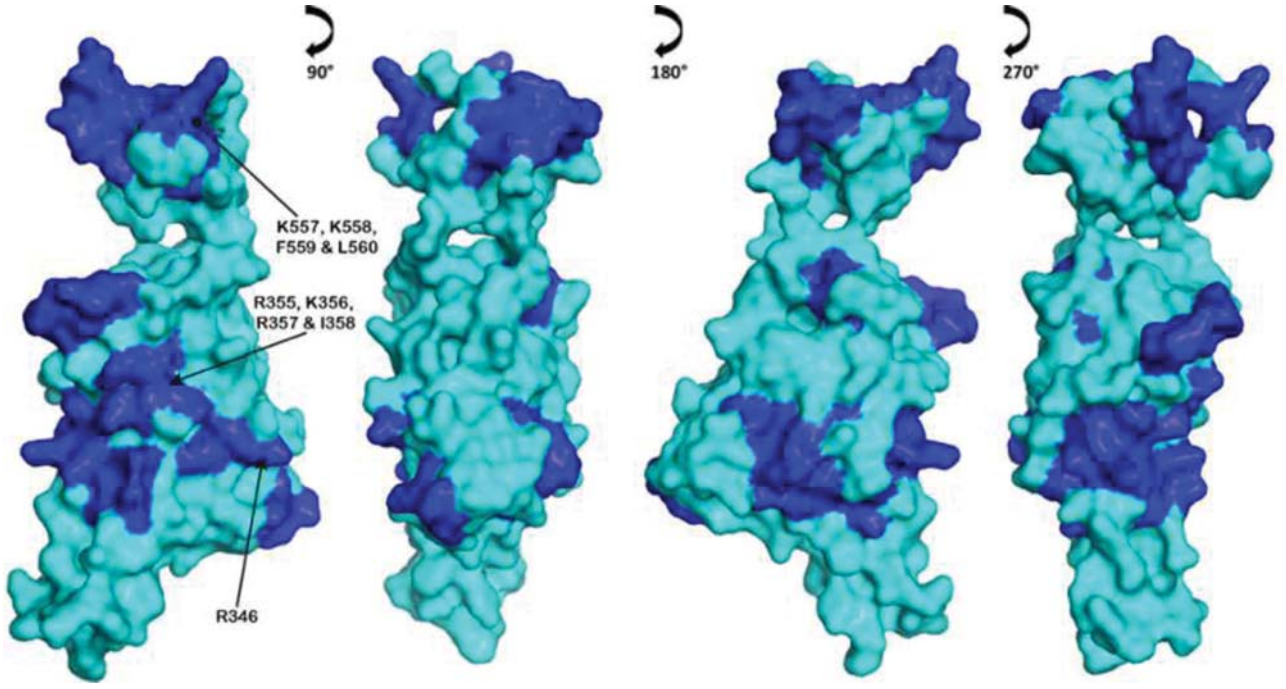

Fig. 7 SARS-CoV-2 S1 RBD protein model. Basic amino acids that are solvent accessible on the surface are indicated (*dark blue*); these form extensive patches. Sequences with the highest normalised count (►**Tables 2** and **3**) are highlighted. R346 is also shown as it indicates a potential heparin-binding gain of function mutation (T346R) from the Bat-RaTG13. RBD, receptor-binding domain.

Table 2 Sequence analysis of SARS-CoV-2 S1 RBD (330–583)

AA No.	330	331	332	333	334	335	336	337	338	339	340	341	342	343	344	345	346	347	348	349	350	351	352	353	354	355	356	357	358	359	360
AA	P	N	I	T	N	L	C	P	F	G	E	V	F	N	A	T	R	F	A	S	V	Y	A	W	N	R	K	R	I	S	N
HBP	0.022	0.000	0.000	0.000	0.000	0.000	0.000	0.000	0.000	0.000	0.000	0.000	0.000	0.000	0.000	0.000	0.368	0.368	0.368	0.000	0.000	0.000	0.000	0.000	0.000	0.941	0.941	0.941	0.941	0.000	0.000
AA No.	361	362	363	364	365	366	367	368	369	370	371	372	373	374	375	376	377	378	379	380	381	382	383	384	385	386	387	388	389	390	391
AA	C	V	A	D	Y	S	V	L	Y	N	S	A	S	F	S	T	F	K	C	Y	G	V	S	P	T	K	L	N	D	L	C
HBP	0.000	0.000	0.000	0.000	0.000	0.000	0.000	0.000	0.000	0.000	0.000	0.000	0.000	0.000	0.000	0.000	0.000	0.000	0.000	0.000	0.000	0.000	0.000	0.000	0.081	0.081	0.081	0.081	0.000	0.000	0.000
AA No.	392	393	394	395	396	397	398	399	400	401	402	403	404	405	406	407	408	409	410	411	412	413	414	415	416	417	418	419	420	421	422
AA	F	T	N	V	Y	A	D	S	F	V	I	R	G	D	E	V	R	Q	I	A	P	G	Q	T	G	K	I	A	D	Y	N
HBP	0.000	0.000	0.000	0.000	0.000	0.000	0.000	0.000	0.386	0.386	0.386	0.386	0.004	0.169	0.169	0.173	0.173	0.004	0.004	0.004	0.000	0.000	0.000	0.000	0.088	0.309	0.309	0.309	0.007	0.015	0.007
AA No.	423	424	425	426	427	428	429	430	431	432	433	434	435	436	437	438	439	440	441	442	443	444	445	446	447	448	449	450	451	452	453
AA	Y	K	L	P	D	D	F	T	G	C	V	I	A	W	N	S	N	N	L	D	S	K	V	G	G	N	Y	N	Y	L	Y
HBP	0.235	0.235	0.235	0.066	0.000	0.000	0.000	0.000	0.000	0.000	0.000	0.000	0.000	0.000	0.000	0.000	0.000	0.000	0.000	0.000	0.063	0.114	0.114	0.051	0.051	0.000	0.000	0.000	0.000	0.000	0.000
AA No.	454	455	456	457	458	459	460	461	462	463	464	465	466	467	468	469	470	471	472	473	474	475	476	477	478	479	480	481	482	483	484
AA	R	L	F	R	K	S	N	L	K	P	F	E	R	D	I	S	T	E	I	Y	Q	A	G	S	T	P	C	N	G	V	E
HBP	0.000	0.000	0.000	0.000	0.000	0.000	0.000	0.110	0.110	0.110	0.114	0.004	0.004	0.004	0.004	0.000	0.000	0.000	0.000	0.000	0.000	0.000	0.000	0.000	0.000	0.000	0.000	0.000	0.000	0.000	0.000
AA No.	485	486	487	488	489	490	491	492	493	494	495	496	497	498	499	500	501	502	503	504	505	506	507	508	509	510	511	512	513	514	515
AA	G	F	N	C	Y	F	P	L	Q	S	Y	G	F	Q	P	T	N	G	V	G	Y	Q	P	Y	R	V	V	V	L	S	F
HBP	0.000	0.000	0.000	0.000	0.000	0.000	0.000	0.000	0.000	0.000	0.000	0.000	0.000	0.000	0.000	0.000	0.000	0.000	0.000	0.000	0.000	0.000	0.015	0.029	0.029	0.029	0.029	0.029	0.029	0.000	0.000
AA No.	516	517	518	519	520	521	522	523	524	525	526	527	528	529	530	531	532	533	534	535	536	537	538	539	540	541	542	543	544	545	546
AA	E	L	L	H	A	P	A	T	V	C	G	P	K	K	S	T	N	L	V	K	N	K	C	V	N	F	N	F	N	G	L
HBP	0.000	0.305	0.305	0.305	0.305	0.004	0.004	0.000	0.000	0.000	0.000	0.000	0.000	0.000	0.000	0.000	0.000	1.000	1.000	1.000	0.000	0.015	0.015	0.015	0.000	0.000	0.000	0.000	0.000	0.000	0.000
AA No.	547	548	549	550	551	552	553	554	555	556	557	558	559	560	561	562	563	564	565	566	567	568	569	570	571	572	573	574	575	576	577
AA	T	G	T	G	V	L	T	E	S	N	K	K	F	L	P	F	Q	Q	F	G	R	D	I	A	D	T	T	D	A	V	R
HBP	0.000	0.000	0.000	0.000	0.000	0.000	0.000	0.000	0.000	0.000	0.544	0.544	0.544	0.544	0.000	0.000	0.000	0.000	0.026	0.026	0.033	0.007	0.007	0.007	0.007	0.000	0.000	0.011	0.688	0.688	0.688
AA No.	578	579	580	581	582	583																									
AA	D	P	Q	T	L	E																									
HBP	0.011	0.000	0.000	0.000	0.000	0.000																									

Abbreviations: AA No; amino acid number. AA; amino acid identity. HBP; relative frequency of sequence among heparin-binding proteins; RBD, receptor-binding domain.
Note: This table shows the amino acid sequence, number, and normalized count for similar sequences in the SARS-CoV-2 RBD as found in a library of 776 heparin-binding proteins. The higher the value, the more often the short heparin-binding sequence was identified among the set of heparin-binding proteins. Basic amino acids within regions of high similarity are identified; arginine (blue), lysine (red), and histidine (green).

Table 3 Predicted heparin-binding domains in SARS-CoV-2 S1 RBD (330–583)

	330	331	332	333	334	335	336	337	338	339	340	341	342	343	344	345	346	347	348	349	350	351	352	353	354	355	356	357	358	359
Human – SARS-CoV-2	P	N	I	T	N	L	C	P	F	G	E	V	F	N	A	T	R	F	A	S	V	Y	A	W	N	R	K	R	I	S
Bat – RaTG13	P	N	I	T	N	L	C	P	F	G	E	V	F	N	A	T	T	F	A	S	V	Y	A	W	N	R	K	R	I	S
Human – SARS-CoV	P	N	I	T	N	L	C	P	F	G	E	V	F	N	A	T	T	F	P	S	V	Y	A	W	E	R	K	R	I	S
Bat – SARS-CoV-related	P	N	I	T	N	L	C	P	F	G	E	V	F	N	A	T	K	F	P	S	V	Y	A	W	E	R	K	K	I	S
Bat – SARS-CoV-related	P	N	I	T	N	L	C	P	F	G	E	V	F	N	A	T	T	F	P	S	V	Y	A	W	E	R	K	R	I	S
	0.022	0	0	0	0	0	0	0	0	0	0	0	0	0	0	0	0.368	0.368	0.368	0	0	0	0	0	0	0.941	0.941	0.941	0.941	0
	360	361	362	363	364	365	366	367	368	369	370	371	372	373	374	375	376	377	378	379	380	381	382	383	384	385	386	387	388	389
Human – SARS-CoV-2	N	C	V	A	D	Y	S	V	L	Y	N	S	A	S	F	S	T	F	K	C	Y	G	V	S	P	T	K	L	N	D
Bat – RaTG13	N	C	V	A	D	Y	S	V	L	Y	N	S	T	S	F	S	T	F	K	C	Y	G	V	S	P	T	K	L	N	D
Human – SARS-CoV	N	C	V	A	D	Y	S	V	L	Y	N	S	T	S	F	S	T	F	K	C	Y	G	V	S	A	T	K	L	N	D
Bat – SARS-CoV-related	N	C	V	A	D	Y	S	V	L	Y	N	S	T	F	F	S	T	F	K	C	Y	G	V	S	A	T	K	L	N	D
Bat – SARS-CoV-related	N	C	V	A	D	Y	S	V	L	Y	N	S	T	S	F	S	T	F	K	C	Y	G	V	S	A	T	K	L	N	D
	0	0	0	0	0	0	0	0	0	0	0	0	0	0	0	0	0	0	0	0	0	0	0	0	0	0.081	0.081	0.081	0.081	0
	390	391	392	393	394	395	396	397	398	399	400	401	402	403	404	405	406	407	408	409	410	411	412	413	414	415	416	417	418	419
Human – SARS-CoV-2	L	C	F	T	N	V	Y	A	D	S	F	V	I	R	G	D	E	V	R	Q	I	A	P	G	Q	T	G	K	I	A
Bat – RaTG13	L	C	F	T	N	V	Y	A	D	S	F	V	I	T	G	D	E	V	R	Q	I	A	P	G	Q	T	G	K	I	A
Human – SARS-CoV	L	C	F	S	N	V	Y	A	D	S	F	V	V	K	G	D	D	V	R	Q	I	A	P	G	Q	T	G	V	I	A
Bat – SARS-CoV-related	L	C	F	S	N	V	Y	A	D	S	F	V	V	K	G	D	D	V	R	Q	I	A	P	G	Q	T	G	V	I	A
Bat – SARS-CoV-related	L	C	F	S	N	V	Y	A	D	S	F	V	V	K	G	D	D	V	R	Q	I	A	P	G	Q	T	G	V	I	A
	0	0	0	0	0	0	0	0	0	0	0.386	0.386	0.386	0.386	0.004	0.169	0.169	0.173	0.173	0.004	0.004	0.004	0	0	0	0	0.088	0.309	0.309	0.309
	420	421	422	423	424	425	426	427	428	429	430	431	432	433	434	435	436	437	438	439	440	441	442	443	444	445	446	447	448	449
Human – SARS-CoV-2	D	Y	N	Y	K	L	P	D	D	F	T	G	C	V	I	A	W	N	S	N	N	L	D	S	K	V	G	G	N	Y
Bat – RaTG13	D	Y	N	Y	K	L	P	D	D	F	T	G	C	V	I	A	W	N	S	K	H	I	D	A	K	E	G	G	N	F
Human – SARS-CoV	D	Y	N	Y	K	L	P	D	D	F	M	G	C	V	L	A	W	N	T	R	N	I	D	A	T	S	T	G	N	Y
Bat – SARS-CoV-related	D	Y	N	Y	K	L	P	D	D	F	M	G	C	V	L	A	W	N	T	R	N	I	D	A	T	S	T	G	N	Y
Bat – SARS-CoV-related	D	Y	N	Y	K	L	P	D	D	F	L	G	C	V	L	A	W	N	T	N	S	K	D	S	S	T	S	G	N	Y
	0.007	0.015	0.007	0.235	0.235	0.235	0.066	0	0	0	0	0	0	0	0	0	0	0	0	0	0	0	0	0.063	0.114	0.114	0.051	0.051	0	0
	450	451	452	453	454	455	456	457	458	459	460	461	462	463	464	465	466	467	468	469	470	471	472	473	474	475	476	477	478	479
Human – SARS-CoV-2	N	Y	L	Y	R	L	F	R	K	S	N	L	K	P	F	E	R	D	I	S	T	E	I	Y	Q	A	G	S	T	P
Bat – RaTG13	N	Y	L	Y	R	L	F	R	K	A	N	L	K	P	F	E	R	D	I	S	T	E	I	Y	Q	A	G	S	K	P
Human – SARS-CoV	N	Y	K	Y	R	S	L	R	H	G	K	L	R	P	F	E	R	D	I	S	N	V	P	F	S	P	D	G	K	P
Bat – SARS-CoV-related	N	Y	K	Y	R	Y	L	R	H	G	K	L	R	P	F	E	R	D	I	S	N	V	P	F	S	P	D	G	K	P
Bat – SARS-CoV-related	N	Y	L	Y	R	W	V	R	R	S	K	L	N	P	Y	E	R	D	L	S	N	D	I	Y	S	P	G	G	Q	S
	0	0	0	0	0	0	0	0	0	0	0	0.110	0.110	0.110	0.114	0.004	0.004	0.004	0.004	0	0	0	0	0	0	0	0	0	0	0
	480	481	482	483	484	485	486	487	488	489	490	491	492	493	494	495	496	497	498	499	500	501	502	503	504	505	506	507	508	509
Human – SARS-CoV-2	C	N	G	V	E	G	F	N	C	Y	F	P	L	Q	S	Y	G	F	Q	P	T	N	G	V	G	Y	Q	P	Y	R
Bat – RaTG13	C	N	G	Q	T	G	L	N	C	Y	Y	P	L	Y	R	Y	G	F	Y	P	T	D	G	V	G	H	Q	P	Y	R
Human – SARS-CoV	C	T	P	P	–	A	F	N	C	Y	W	P	L	N	D	Y	G	F	F	T	T	N	G	I	G	Y	Q	P	Y	R
Bat – SARS-CoV-related	C	T	P	P	–	A	L	N	C	Y	W	P	L	N	D	Y	G	F	Y	T	T	T	G	I	G	Y	Q	P	Y	R
Bat – SARS-CoV-related	C	S	A	I	–	G	P	N	C	Y	N	P	L	R	P	Y	G	F	F	T	T	A	G	V	G	H	Q	P	Y	R
	0	0	0	0	0	0	0	0	0	0	0	0	0	0	0	0	0	0	0	0	0	0	0	0	0	0	0	0.015	0.029	0.029
	510	511	512	513	514	515	516	517	518	519	520	521	522	523	524	525	526	527	528	529	530	531	532	533	534	535	536	537	538	539
Human – SARS-CoV-2	V	V	V	L	S	F	E	L	L	H	A	P	A	T	V	C	G	P	K	K	S	T	N	L	V	K	N	K	C	V

Table 3 (*Continued*)

	330	331	332	333	334	335	336	337	338	339	340	341	342	343	344	345	346	347	348	349	350	351	352	353	354	355	356	357	358	359
Bat – RaTG13	V	V	V	L	S	F	E	L	L	N	A	P	A	T	V	C	G	P	K	K	S	T	N	L	V	K	N	K	C	V
Human – SARS-CoV	V	V	V	L	S	F	E	L	L	N	A	P	A	T	V	C	G	P	K	L	S	T	D	L	I	K	N	Q	C	V
Bat – SARS-CoV-related	V	V	V	L	S	F	E	L	L	N	A	P	A	T	V	C	G	P	K	L	S	T	D	L	I	K	N	Q	C	V
Bat – SARS-CoV-related	V	V	V	L	S	F	E	L	L	N	A	P	A	T	V	C	G	P	K	L	S	T	D	L	I	K	N	Q	C	V
	0.029	0.029	0.029	0.029	0	0	0	0.305	0.305	0.305	0.305	0.004	0.004	0	0	0	0	0	0	0	0	0	0	1.000	1.000	1.000	0.000	0.015	0.015	0.015
	540	541	542	543	544	545	546	547	548	549	550	551	552	553	554	555	556	557	558	559	560	561	562	563	564	565	566	567	568	569
Human – SARS-CoV-2	N	F	N	F	N	G	L	T	G	T	G	V	L	T	E	S	N	K	K	F	L	P	F	Q	Q	F	G	R	D	I
Bat – RaTG13	N	F	N	F	N	G	L	T	G	T	G	V	L	T	E	S	N	K	K	F	L	P	F	Q	Q	F	G	R	D	I
Human – SARS-CoV	N	F	N	F	N	G	L	T	G	T	G	V	L	T	P	S	S	K	R	F	Q	P	F	Q	Q	F	G	R	D	V
Bat – SARS-CoV-related	N	F	N	F	N	G	L	T	G	T	G	V	L	T	P	S	S	K	R	F	Q	P	F	Q	Q	F	G	R	D	V
Bat – SARS-CoV-related	N	F	N	F	N	G	L	T	G	T	G	V	L	T	S	S	S	K	R	F	Q	P	F	Q	Q	F	G	R	D	V
	0	0	0	0	0	0	0	0	0	0	0	0	0	0	0	0	0	0.544	0.544	0.544	0.544	0	0	0	0	0.026	0.026	0.033	0.007	0.007
	570	571	572	573	574	575	576	577	578	579	580	581	582	583																
Human – SARS-CoV-2	A	D	T	T	D	A	V	R	D	P	Q	T	L	E																
Bat – RaTG13	A	D	T	T	D	A	V	R	D	P	Q	T	L	E																
Human – SARS-CoV	S	D	F	T	D	S	V	R	D	P	K	T	S	E																
Bat – SARS-CoV-related	S	D	F	T	D	S	V	R	D	P	K	T	S	E																
Bat – SARS-CoV-related	S	D	F	T	D	S	V	R	D	P	K	T	S	E																
	0.007	0.007	0	0	0.011	0.688	0.688	0.688	0.011	0	0	0	0	0																

Abbreviation: SARS-CoV, severe acute respiratory syndrome coronavirus.

Note: This table shows the amino acid sequence, number, and normalized count for similar short, heparin-binding sequences in the SARS-CoV-2 RBD found in a library of 776 heparin binding proteins. In addition to SARS-CoV-2, the table also contains the aligned sequences from similar viruses, SARS-CoV, and related bat viruses. The predicted heparin-binding regions are shown in yellow and variations within those regions between SARS-CoV-2 and the related viruses are highlighted in red.

Molecular Modelling of SARS-CoV-2 RBD and Heparin Oligosaccharides

To evaluate the basic residue clusters obtained from the bioinformatics analyses, we used systematic docking calculations that searched the entire protein surface of SARS-CoV-2 RBD, using models of heparin tetrasaccharide as probes. ClusPro results are in agreement with the results shown in ►**Tables 2** and **3**, indicating the presence of four basic heparin-binding clusters, here onwards referred to as sites I, II and III. Docking of multiple tetrasaccharides indicates the presence of a binding site consisting of residues K356, R357, R355, R466, R346, K444 and R509 (site I). The distances between various residues indicate that site I could bind a heparin oligosaccharide longer than dp6 (►**Supplementary Fig. S1**, available in the online version). Site II comprises the region around basic residues R457, K458 and K462 and could accommodate a heparin tetrasaccharide (►**Supplementary Fig. S1**, available in the online version). Site III is adjacent to the ACE2 interface and comprises residues R408, R403 and K417 (►**Supplementary Fig. S2**, available in the online version). In the absence of glycosylation and other domains of S1, ClusPro analyses of the truncated structure (PDB:6ZGG; chain B) identified residues LVK 533–535 and KK 557–558 of subdomain 1 (SD1) as heparin tetrasaccharide binding sites (data not shown), which agrees with the sequence analysis above.

The results for the docking of a heparin octasaccharide, using GlycoTorch Vina, revealed that the entire oligosaccharide has favourable affinity for site I (docking score = −5.4 kcal/mol) whereas the same octasaccharide showed unfavourable preference for site III. Docking of a heparin hexasaccharide indicates that site III (►►**Supplementary Fig. S4**, available in the online version) can accommodate heparin fragments equal or shorter than a hexasaccharide. The obtained docking results confirmed that the binding of heparin fragments to sites I, II and III is length-dependent.

To explore the key binding residues that may play an important role in binding to the SARS-CoV-2 RBD region, the intermolecular interactions between the heparin oligosaccharides and the protein residues were quantified from the MD trajectories using the pairwise per residue decomposition energy module in AMBER. Amino acid residues found to be of importance for interacting with a heparin octasaccharide were T345, R346, N354, R355, K356, R357, I358, S359, L441, D442, K444, N448, Y449, N450, R466 and R509 (►**Fig. 8A**). The strength of these interactions varied from −1.0 to −17.5 kcal/mol. The interactions between a heparin hexasaccharide and site III of RBD was also examined, demonstrating a favourable interaction with residues R403, R408, N409, T415, G416, K417, Y421, N501 and Y505 (►**Fig. 8B**) and a strength of interactions in the range of −1.0 to −10 kcal/mol. The interactions of heparin with residues D405-E406 are unfavourable due to the negative charge.

Conformational change in the SARS-CoV-2 spike RBD using 500 nanosecond MD simulations was investigated using the DSSP (Define Secondary Structure of Proteins) program implemented in AmberTools. Changes in the secondary structure elements of the RBD in the presence of heparin oligosaccharides trajectory are shown in ►**Supplementary Fig. S3** (available in the online version). The β-sheets maintain the most stable regions of secondary structure, whereas the α- and 3_{10}-helices, turns and loops connecting the β-sheets, undergo conformational change in both systems. The C-terminal of the RBD domain is connected to the SD1 domain through a long flexible loop (residues A520–K535). This will further contribute to a conformational change in the system upon binding of oligosaccharides.

Heparin-interacting residues Y449, K417, Y505, N501 and G502 of the RBD are also hotspots for ACE2 receptor binding

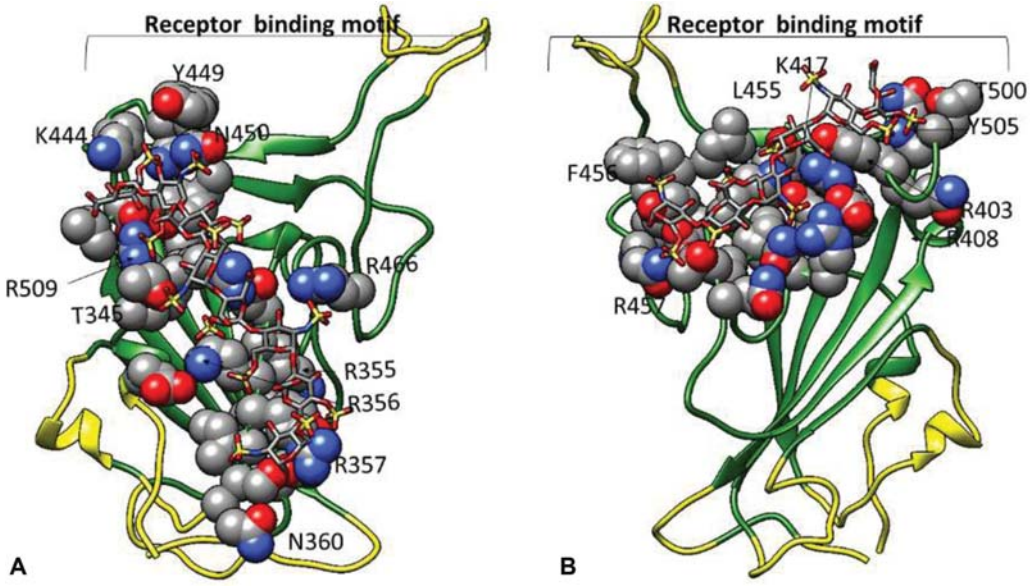

Fig. 8 Snapshots taken from MD simulations of SARS-CoV-RBD in the presence of either a heparin octasaccharide (A) or a heparin hexasaccharide (**B**). The heparin oligosaccharides are shown as sticks whereas amino acids of the RBD are shown as spheres. The residues are coloured as per elements. Hydrogen atoms are not shown for clarity. The regions subjected to conformational changes in the protein during the simulations are highlighted in yellow ribbon. MD, molecular dynamics; RBD, receptor-binding domain.

(known as the receptor-binding motif). This complements the experimental data showing that heparin binding induces a conformational change and inhibits the binding of ACE2.

Discussion and Conclusion

The rapid spread of SARS-CoV-2 represents a significant challenge to global health authorities. Moreover, it is likely that humanity will face future epidemics. Therefore, strategies are required for treatments that might reduce the burden of disease. Basing therapeutics on fundamental aspects of the biology of pathogen–host interactions that will be reasonably constant at the molecular level would provide the means to develop treatments in the face of new, rapidly spreading pathogens, such as SARS-CoV-2. The interaction of a sizable number of pathogens, including the *Coronaviridae* with peri- and extracellular HS, represents such an opportunity.

Glycosaminoglycans such as HS are present on almost all animal cells and this class of carbohydrates is central to the strategy employed by numerous pathogens,[46,47] including the *Coronaviridae*,[48] to attach to host cells. It is likely that the host has a very limited ability to alter HS structures employed by the pathogen. This is due to at least two factors. First, the large number of protein partners of HS,[2,5,7] each showing some level of selectivity for different saccharide structures. Second, binding specificity is selective for patterns of charged groups in a particular geometry, which are attainable by different saccharide sequences.[49] The consequence is a high degree of degeneracy and selectivity of proteins for HS, but never absolute specificity, i.e., one protein, one saccharide sequence.[7,44] However, on the pathogen's part, there are also restrictions. In the case of viruses, their limited repertoire of extracellular proteins may result in overlapping binding sites. The likely overlap of the ACE2 site in SARS-Cov-2 S1 RBD with its predicted heparin (likewise HS) binding site being one example. Thus, HS presents a reasonably constant molecular target for a pathogen, which in turn offers unique therapeutic possibilities, as illustrated in the present work.

Our initial observation of an interaction between SARS-CoV-2 S1 RBD and heparin[50] has now been confirmed by subsequent work.[51,52] Here, we show that this interaction is associated with an inhibition by heparin of cell invasion by SARS-CoV-2, in a dose-dependent manner at concentrations from 6.25 to 200 μg mL^{-1}, up to 80% in Vero cells, concentrations within the range experienced during anticoagulation therapy. Furthermore, host cell surface GAGs are likely to act as SARS-CoV-2 binding sites, as the addition of exogenous heparin disrupted RBD binding to the cell surface. These data suggest that heparin, or one of its derivatives, may be effective in controlling infection by SARS-CoV-2. Moreover, infections by the *Coronaviridae* including SARS-CoV-2 are often accompanied by marked coagulopathy, which is the usual clinical target of heparin.[53] There are also data to suggest that heparin can modulate excessive inflammatory responses,[54,55] and these are another hallmark of SARS-CoV-2 infections.

Protective effects of heparin in COVID-19 patients have been described[53] as research begins to reveal the mechanism behind increased clotting during the disease. Although promising, questions concerning the timing of treatment, the appropriate dosage and the selection of anticoagulation therapy remain unanswered.[56] In addition, there is the possibility of targeting with heparin directly the luminal surface of the respiratory tract both to reduce infectivity on this surface and thromboses in the air sacs, through the delivery of nebulised heparin. This is a strategy behind two clinical trials.[38]

The present data provide direct evidence for the pursuit of the CHARTER and COVID-19 HOPE trials.[38] Moreover, together with the many prior studies on the interactions of pathogens with host GAGs, they suggest that this apparent Achilles' heel of the host may be exploited therapeutically in a range of infectious diseases using heparin and its derivatives, drugs that are readily available and cheap world-wide, and which are well tolerated even in extremely ill patients.

What is known about this topic?

- The coronavirus SARS-CoV-2 is the causative agent of COVID-19.
- The pandemic COVID-19 disease is of global significance and an international health emergency.
- The SARS-CoV-2 spike protein is responsible for host cell attachment and invasion.
- The SARS-CoV-2 spike S1 receptor-binding domain (RBD) is known to bind to human angiotensin I converting enzyme 2 (ACE2) and this is believed to facilitate host cell invasion.
- Heparin has been shown previously by the authors to inhibit viral invasion by the historical S-associated coronavirus HSR strain [responsible for infections in the original 2002–2004 severe acute respiratory syndrome (SARS) outbreak], although the potency of inhibition for this coronavirus was not believed to be of therapeutic significance.

What does this paper add?

This manuscript demonstrates for the first time that:

- Heparin inhibits cellular invasion of SARS-CoV-2 coronavirus in live virus assays and this inhibition is significantly more potent than that of historical coronavirus strains.
- The inhibition of live virus by heparin occurs at concentrations that would enable therapeutic use, unlike those observed for historical SARS-causing coronavirus strains.
- Heparin blocks the binding of recombinantly expressed SARS-CoV-2 spike S1 RBD protein to pathologically relevant Vero cells.
- Heparin binds to the SARS-CoV-2 spike S1 RBD and this manuscript highlights the structural dependencies with regard to heparin.
- The interaction of heparin with SARS-CoV-2 spike S1 RBD induces a conformational change in the SARS-CoV-2 spike S1 RBD protein.

Funding
This study was funded by the Biotechnology and Biological Sciences Research Council, UK (BB/L023717/1; BIV-HVB-2020/07/SKIDMORE; BB/S009787/1) and the Fundação de Amparo à Pesquisa do Estado de São Paulo, Brazil (2020/04899-1).

Conflict of Interest
None declared.

References

1 Woznica A, Gerdt JP, Hulett RE, Clardy J, King N. Mating in the closest living relatives of animals is induced by a bacterial chondroitinase. Cell 2017;170(06):1175.e11–1183.e11
2 Ori A, Wilkinson MC, Fernig DG. A systems biology approach for the investigation of the heparin/heparan sulfate interactome. J Biol Chem 2011;286(22):19892–19904
3 Ireland EV, Woznica A, King N. Synergistic cues from diverse bacteria enhance multicellular development in a choanoflagellate. Appl Environ Microbiol 2020;86(11):e02920-19
4 Ori A, Wilkinson MC, Fernig DG. The heparanome and regulation of cell function: structures, functions and challenges. Front Biosci 2008;13:4309–4338
5 Nunes QM, Su D, Brownridge PJ, et al. The heparin-binding proteome in normal pancreas and murine experimental acute pancreatitis. PLoS One 2019;14(06):e0217633
6 Rudd TR, Preston MD, Yates EA. The nature of the conserved basic amino acid sequences found among 437 heparin binding proteins determined by network analysis. Mol Biosyst 2017;13(05):852–865
7 Meneghetti MCZ, Hughes AJ, Rudd TR, et al. Heparan sulfate and heparin interactions with proteins. J R Soc Interface 2015;12 (110):0589
8 Cagno V, Tseligka ED, Jones ST, Tapparel C. Heparan sulfate proteoglycans and viral attachment: true receptors or adaptation bias? Viruses 2019;11(07):596
9 Chandra N, Liu Y, Liu JX, et al. Sulfated glycosaminoglycans as viral decoy receptors for human adenovirus type 37. Viruses 2019;11 (03):247
10 Xu D, Esko JD. Demystifying heparan sulfate-protein interactions. Annu Rev Biochem 2014;83:129–157
11 Vicenzi E, Canducci F, Pinna D, et al. Coronaviridae and SARS-associated coronavirus strain HSR1. Emerg Infect Dis 2004;10 (03):413–418
12 Vicenzi E, Pagani I, Ghezzi S, et al. Subverting the mechanisms of cell death: flavivirus manipulation of host cell responses to infection. Biochem Soc Trans 2018;46(03):609–617
13 Ghezzi S, Cooper L, Rubio A, et al. Heparin prevents Zika virus induced-cytopathic effects in human neural progenitor cells. Antiviral Res 2017;140:13–17
14 WuDunn D, Spear PG. Initial interaction of herpes simplex virus with cells is binding to heparan sulfate. J Virol 1989;63(01):52–58
15 Skidmore MA, Kajaste-Rudnitski A, Wells NM, et al. Inhibition of influenza H5N1 invasion by modified heparin derivatives. MedChemComm 2015;6:640–646
16 Rusnati M, Coltrini D, Oreste P, et al. Interaction of HIV-1 Tat protein with heparin. Role of the backbone structure, sulfation, and size. J Biol Chem 1997;272(17):11313–11320
17 Harrop HA, Rider CC. Heparin and its derivatives bind to HIV-1 recombinant envelope glycoproteins, rather than to recombinant HIV-1 receptor, CD4. Glycobiology 1998;8(02):131–137
18 Clementi N, Criscuolo E, Diotti RA, et al. Combined prophylactic and therapeutic use maximizes hydroxychloroquine anti-SARS-CoV-2 effects in vitro. bioRxiv 2020. Doi: 2020.03.29.014407. Accessed November 1, 2020 at: https://www.biorxiv.org/content/10.1101/2020.03.29.014407v1
19 Yates EA, Santini F, Guerrini M, Naggi A, Torri G, Casu B. 1H and 13C NMR spectral assignments of the major sequences of twelve systematically modified heparin derivatives. Carbohydr Res 1996;294:15–27
20 Micsonai A, Wien F, Kernya L, et al. Accurate secondary structure prediction and fold recognition for circular dichroism spectroscopy. Proc Natl Acad Sci U S A 2015;112(24):E3095–E3103
21 Rudd TR, Skidmore MA, Guimond SE, et al. The potential for circular dichroism as an additional facile and sensitive method of monitoring low-molecular-weight heparins and heparinoids. Thromb Haemost 2009;102(05):874–878
22 Rudd TR, Guimond SE, Skidmore MA, et al. Influence of substitution pattern and cation binding on conformation and activity in heparin derivatives. Glycobiology 2007;17(09):983–993
23 Duchesne L, Gentili D, Comes-Franchini M, Fernig DG. Robust ligand shells for biological applications of gold nanoparticles. Langmuir 2008;24(23):13572–13580
24 Thakar D, Migliorini E, Coche-Guerente L, et al. A quartz crystal microbalance method to study the terminal functionalization of glycosaminoglycans. Chem Commun (Camb) 2014;50(96): 15148–15151
25 Migliorini E, Thakar D, Sadir R, et al. Well-defined biomimetic surfaces to characterize glycosaminoglycan-mediated interactions on the molecular, supramolecular and cellular levels. Biomaterials 2014;35(32):8903–8915
26 Wang Q, Zhang Y, Wu L, et al. Structural and functional basis of SARS-CoV-2 entry by using human ACE2. Cell 2020;181(04):894. e9–904.e9
27 Lan J, Ge J, Yu J, et al. Structure of the SARS-CoV-2 spike receptor-binding domain bound to the ACE2 receptor. Nature 2020;581 (7807):215–220
28 Boittier E, Burns JM, Gandhi NS, et al. GlycoTorch vina: improved docking of sulfated sugars using QM-derived scoring functions. 2020. Accessed November 1, 2020 at: https://chemrxiv.org/articles/preprint/GlycoTorch_Vina_Improved_Docking_of_Sulfated_Sugars_Using_QM-derived_Scoring_Functions/12279251
29 Best RB, Hummer G. Optimized molecular dynamics force fields applied to the helix-coil transition of polypeptides. J Phys Chem B 2009;113(26):9004–9015
30 Kirschner KN, Yongye AB, Tschampel SM, et al. GLYCAM06: a generalizable biomolecular force field. Carbohydrates. J Comput Chem 2008;29(04):622–655
31 Jorgensen WL, Chandrasekhar J, Madura JD, et al. Comparison of simple potential functions for simulating liquid water. J Chem Phys 1983;79:926–935
32 Case DA, Cerutti DS, Cheatham TEI, et al. Amber 2017 Reference Manual. Univ. CaliforniaSan Francisco2017. Accessed November 1, 2020 at: http://ambermd.org/doc12/Amber17.pdf
33 Pettersen EF, Goddard TD, Huang CC, et al. UCSF Chimera–a visualization system for exploratory research and analysis. J Comput Chem 2004;25(13):1605–1612
34 Dolinsky TJ, Nielsen JE, McCammon JA, Baker NA. PDB2PQR: an automated pipeline for the setup of Poisson-Boltzmann electrostatics calculations. Nucleic Acids Res 2004;32(Web Server issue):W665-7
35 Onufriev A, Bashford D, Case DA. Exploring protein native states and large-scale conformational changes with a modified generalized born model. Proteins 2004;55(02):383–394
36 Weiser J, Shenkin PS, Still WC. Approximate atomic surfaces from linear combinations of pairwise overlaps (LCPO). J Comput Chem 1999;20:217–230
37 Genheden S, Ryde U. The MM/PBSA and MM/GBSA methods to estimate ligand-binding affinities. Expert Opin Drug Discov 2015; 10(05):449–461
38 Dixon B, Smith R, Artigas A, et al. Can nebulised heparin reduce time to extubation in SARS CoV 2 the CHARTER study protocol. medRxiv 2020. Doi: 2020.04.28.20082552. Accessed November 1, 2020 at: http://medrxiv.org/lookup/doi/10.1101/2020.04.28.20082552

39 Schmith VD, Zhou JJ, Lohmer LRL. The approved dose of ivermectin alone is not the ideal dose for the treatment of COVID-19. Clin Pharmacol Ther 2020;108(04):762–765

40 Duchesne L, Octeau V, Bearon RN, et al. Transport of fibroblast growth factor 2 in the pericellular matrix is controlled by the spatial distribution of its binding sites in heparan sulfate. PLoS Biol 2012;10(07):e1001361

41 Schuck P, Zhao H. The role of mass transport limitation and surface heterogeneity in the biophysical characterization of macromolecular binding processes by SPR biosensing. Methods Mol Biol 2010;627:15–54

42 Sadir R, Forest E, Lortat-Jacob H. The heparan sulfate binding sequence of interferon-γ increased the on rate of the interferon-γ-interferon-γ receptor complex formation. J Biol Chem 1998;273 (18):10919–10925

43 Yates EA, Santini F, De Cristofano B, et al. Effect of substitution pattern on 1H, 13C NMR chemical shifts and 1J(CH) coupling constants in heparin derivatives. Carbohydr Res 2000;329(01): 239–247

44 Rudd TR, Yates EA. Conformational degeneracy restricts the effective information content of heparan sulfate. Mol Biosyst 2010;6(05):902–908

45 Lima MA, Hughes AJ, Veraldi N, et al. Antithrombin stabilisation by sulfated carbohydrates correlates with anticoagulant activity. MedChemComm 2013;4:870–873

46 Chang YC, Wang Z, Flax LA, et al. Glycosaminoglycan binding facilitates entry of a bacterial pathogen into central nervous systems. PLoS Pathog 2011;7(06):e1002082

47 García B, Merayo-Lloves J, Martin C, Alcalde I, Quirós LM, Vazquez F. Surface proteoglycans as mediators in bacterial pathogens infections. Front Microbiol 2016;7:220

48 Milewska A, Zarebski M, Nowak P, Stozek K, Potempa J, Pyrc K. Human coronavirus NL63 utilizes heparan sulfate proteoglycans for attachment to target cells. J Virol 2014;88(22):13221–13230

49 Guerrini M, Elli S, Mourier P, et al. An unusual antithrombin-binding heparin octasaccharide with an additional 3-O-sulfated glucosamine in the active pentasaccharide sequence. Biochem J 2013;449(02):343–351

50 Mycroft-West CJ, Su D, Elli S, et al. The 2019 coronavirus (SARS-CoV-2) surface protein (Spike) S1 receptor binding domain undergoes conformational change upon heparin binding. bioRxiv 2020. Accessed November 1, 2020 at: https://doi.org/10.1101/2020.02. 29.971093

51 Liu L, Chopra P, Li X, et al. SARS-CoV-2 spike protein binds heparan sulfate in a length- and sequence-dependent manner. bioRxiv 2020. Doi: 2020.05.10.087288. Accessed November 1, 2020 at: https://doi.org/10.1101/2020.05.10.087288

52 Kim SY, Jin W, Sood A, et al. Glycosaminoglycan binding motif at S1/S2 proteolytic cleavage site on spike glycoprotein may facilitate novel coronavirus (SARS-CoV-2) host cell entry. bioRxiv 2020. Doi: 10.1101/2020.04.14.041459

53 Tang N, Bai H, Chen X, Gong J, Li D, Sun Z. Anticoagulant treatment is associated with decreased mortality in severe coronavirus disease 2019 patients with coagulopathy. J Thromb Haemost 2020;18(05):1094–1099

54 Veraldi N, Hughes AJ, Rudd TR, et al. Heparin derivatives for the targeting of multiple activities in the inflammatory response. Carbohydr Polym 2015;117:400–407

55 Mousavi S, Moradi M, Khorshidahmad T, Motamedi M. Anti-inflammatory effects of heparin and its derivatives: a systematic review. Adv Pharmacol Sci 2015;2015:507151

56 Thachil J. The versatile heparin in COVID-19. J Thromb Haemost 2020;18(05):1020–1022